

3-1-2020

Neutron-hole strength in N=81 nuclei

A. M. Howard
The University of Manchester

S. J. Freeman
The University of Manchester

D. K. Sharp
The University of Manchester

T. Bloxham
University of California, Berkeley

J. A. Clark
Argonne National Laboratory

See next page for additional authors

Follow this and additional works at: https://digitalcommons.lsu.edu/physics_astronomy_pubs

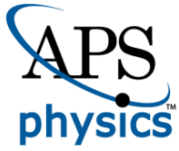
Recommended Citation

Howard, A., Freeman, S., Sharp, D., Bloxham, T., Clark, J., Deibel, C., Kay, B., Parker, P., Schiffer, J., & Thomas, J. (2020). Neutron-hole strength in N=81 nuclei. *Physical Review C*, 101 (3) <https://doi.org/10.1103/PhysRevC.101.034309>

This Article is brought to you for free and open access by the Department of Physics & Astronomy at LSU Digital Commons. It has been accepted for inclusion in Faculty Publications by an authorized administrator of LSU Digital Commons. For more information, please contact ir@lsu.edu.

Authors

A. M. Howard, S. J. Freeman, D. K. Sharp, T. Bloxham, J. A. Clark, C. M. Deibel, B. P. Kay, P. D. Parker, J. P. Schiffer, and J. S. Thomas



CHORUS

This is the accepted manuscript made available via CHORUS. The article has been published as:

Neutron-hole strength in $N=81$ nuclei

A. M. Howard, S. J. Freeman, D. K. Sharp, T. Bloxham, J. A. Clark, C. M. Deibel, B. P. Kay, P. D. Parker, J. P. Schiffer, and J. S. Thomas

Phys. Rev. C **101**, 034309 — Published 20 March 2020

DOI: [10.1103/PhysRevC.101.034309](https://doi.org/10.1103/PhysRevC.101.034309)

Neutron-hole strength in $N = 81$ nuclei

A. M. Howard,^{1,*} S. J. Freeman,^{1,†} D. K. Sharp,¹ T. Bloxham,^{2,3} J. A. Clark,⁴
C. M. Deibel,^{4,5,‡} B. P. Kay,⁴ P. D. Parker,⁶ J. P. Schiffer,⁴ and J. S. Thomas¹

¹*Department of Physics and Astronomy, University of Manchester, Manchester M13 9PL, United Kingdom*

²*Physics Department, University of California, Berkeley, California 94720, USA*

³*Lawrence Berkeley National Laboratory, Berkeley, California 94720, USA*

⁴*Physics Division, Argonne National Laboratory, Argonne, Illinois 60439, USA*

⁵*Joint Institute for Nuclear Astrophysics, Michigan State University, East Lansing, Michigan 48824, USA*

⁶*A. W. Wright Nuclear Structure Laboratory, Yale University, New Haven, Connecticut 06520, USA*

(Dated: February 6, 2020)

A systematic study of neutron-hole strength in the $N = 81$ nuclei ^{137}Ba , ^{139}Ce , ^{141}Nd and ^{143}Sm is reported. The single-neutron removal reactions (p,d) and $(^3\text{He},\alpha)$ were measured at energies of 23 and 34 MeV, respectively. Spectroscopic factors were extracted from measured cross sections through a distorted-wave Born approximation analysis and centroids of single-particle strength have been established. The change in these centroid energies as a function of proton number have been compared to calculations of the monopole shift for the $s_{1/2}$ and $h_{11/2}$ orbitals, where the majority of the strength has been observed. Significant fragmentation of strength was observed for the d and $g_{7/2}$ orbitals, particularly for the latter orbital which is deeply bound, with summed strengths that indicate a significant amount lies outside of the measured excitation energy range.

I. INTRODUCTION

The description of atomic nuclei in terms of constituent nucleons moving within a mean-field potential is the basis of the shell model, and consequently, much of our understanding of nuclear structure. Over the past decade or so, evidence has emerged indicating that, when moving away from stability into exotic systems, the ordering of single-particle levels evolves as a function of proton and neutron number to the extent that the gaps between levels that correspond to shell and sub-shell closures are found to alter. Significant attention has been paid to these phenomena in the literature, which has motivated a careful reexamination of how the interaction between valence protons and neutrons drives such evolution. On moving through a series of isotopes or isotones, the changing single-particle occupancies of one type of nucleon alters the overall effect of interactions with a nucleon of the other type, thus changing its effective single-particle energy. It appears that in some cases both the central and tensor components of the nucleon-nucleon interaction need to be considered carefully in order to reproduce the observed changes in single-particle structure [1–3].

It is therefore interesting to carefully reexamine the trends in single-particle states near the line of β stability, particularly where changes can be tracked across a range of proton-neutron ratios. Such experimental measurements are often easier and tend to yield more detailed information compared to studies with radioactive beams,

which are performed with inevitably lower beam intensities. In many experiments with stable beams, centroids of single-particle strength can be constructed from the observation of several different excited states populated by transfer of a nucleon to the same orbital and used to estimate its effective single-particle energy.

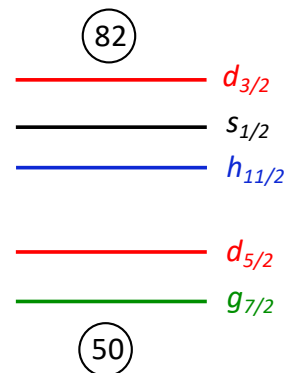


FIG. 1. Schematic level diagram of the single-particle orbitals near stability for the shell between $N = 50$ and $N = 82$.

Several studies have been performed recently using consistent approaches to both experimental and analytical methods that have highlighted the detailed trends in single-particle orbitals in near stable nuclei. These include studies of high- j proton states outside of stable Sn cores [4]; untangling particle-vibration coupling to reveal the underlying neutron orbitals outside $N = 82$ isotones [5, 6]; single-neutron states in $N = 51$ nuclei [7]; and a detailed study of the single-particle properties in Ni isotopes [8, 9].

This paper focusses on a systematic study of hole states in the $N = 82$ closed core. The low-lying structure of

* Current address: FRM-II Heinz Maier-Leibnitz Research Neutron Source, Technical University of Munich, Lichtenbergstrasse 1 85748 Garching Germany.

† Correspondence to: sean.freeman@manchester.ac.uk

‡ Current address: Department of Physics and Astronomy, Louisiana State University, Baton Rouge, LA 70803, USA.

$N = 81$ nuclei is largely based on configurations formed via core coupling with neutron holes in the shell between $N = 50$ and $N = 82$ (see, for example, Reference [10]). This shell is composed of $0g_{7/2}$, $1d_{5/2}$, $1d_{3/2}$, $2s_{1/2}$ and $0h_{11/2}$ single-particle orbitals, shown schematically in Figure 1. The even- Z , $N = 81$ isotopes that can be studied using stable beams and solid targets range from $^{137}_{56}\text{Ba}$ to $^{143}_{62}\text{Sm}$.

Light-ion nucleon-transfer reactions are a traditional tool with which to probe single-particle structure in nuclei and have been used for many years generating a wealth of information in the literature. However, systematic studies across chains of nuclei have been less common in the past and it can be difficult to use isolated studies to evaluate systematic trends as different experimental conditions and techniques have often been employed. In addition, the distorted-wave Born approximation (DWBA) calculations required to extract spectroscopic information have been done with different computing codes and different choices of input parameters in different studies and were often limited by the computation power available at the time, leading to the use of multifarious approximations. Indeed, the researcher trying to reassess experiments in the literature with modern reaction approaches is stymied where the original absolute cross section data are not available in publications and only graphs of relative angular distributions or tables of spectroscopic factors are reported.

Here we describe a series of single-nucleon transfer experiments on stable solid $N = 82$ targets, using a magnetic spectrometer, that have been used to determine the location of single-neutron hole strength in $N = 81$ systems. These employ both the (p,d) and $(^3\text{He},\alpha)$ reactions to ensure good momentum matching for low- and high- ℓ transfers, respectively.

There are several published works in the literature on hole strength, but systematic data across the solid stable $N = 82$ targets using a consistent approach to both the experimental technique and the DWBA calculations with each reaction are not available. The (p,d) reaction has been studied previously on ^{138}Ba , ^{140}Ce , ^{142}Nd and ^{144}Sm targets, but with worse resolution than the current work [11–13]. High-resolution measurements of the $(^3\text{He},\alpha)$ reaction were studied on ^{140}Ce , ^{142}Nd and ^{144}Sm targets in Ref. [14], which also reports measurements of the (d,t) reaction. However, the helium-induced reaction on a ^{138}Ba target has not been studied before. In all this previous work, a zero-range approximation was used in the DWBA calculations and it was noted in several cases that there was sensitivity to some of the associated corrections [11, 12]. The calculations were also normalized by making assumptions about the single-particle purity of the $3/2^+$ ground states in each residual nucleus. Better approaches can now be employed to both DWBA calculations and the determination of their normalization. In addition to these studies, there are also a number of publications of reactions on isolated targets [15–20].

The current publication is organized in the following

manner. Aspects of the experimental methodology will be discussed first, covering neutron removal with both (p,d) and $(^3\text{He},\alpha)$ reactions. The approach used to the DWBA calculations and normalization of the calculated cross sections follows, and the deduced single-neutron energies will then be compared to a simple model based on a two-body effective interaction between protons and neutrons.

II. EXPERIMENTAL DETAILS

Beams of 23-MeV protons and 34-MeV ^3He ions were provided by the tandem Van de Graaff accelerator at the A. W. Wright Nuclear Structure Laboratory of Yale University. These beams were used to bombard targets of ^{138}Ba , ^{140}Ce , ^{142}Nd and ^{144}Sm . Momentum analysis of the ejectile ions was performed using the Yale Enge Split-Pole Spectrograph. At the focal plane, a multiwire gas proportional counter, backed by a plastic scintillator, was used to measure position, energy loss and residual energy of the ions passing through it. The ions were identified by combining information on magnetic rigidity and energy-loss characteristics in the gas detector. The beam dose was measured using a current integrator connected to a tantalum beam stop positioned behind the target. A +300 V bias was applied to both the target frame and beam stop to suppress electron sputtering. Beam currents were typically in the range 50 to 100 enA for each beam species. A 1.5-mm thick silicon detector was mounted at 30° to the beam axis to monitor target thickness, although the ratio of elastic scattering to beam current varied by less than 3% on individual targets during the experiment.

Given the reactivity of the chemical elements used as targets, oxygen is an inevitable contaminant and, to avoid complicated vacuum transfer procedures, targets were manufactured by evaporation of isotopically-enriched oxide material onto supporting carbon foils of thickness $20\text{--}40\mu\text{gcm}^{-2}$. Reactions on oxygen and carbon did not overly complicate the analysis since the kinematic properties of ejectile ions from the contaminant reactions were sufficiently different from those of interest to be easily identified.

To allow the extraction of absolute cross sections, a calibration of the target thickness and spectrograph acceptance was necessary. The product of these two quantities was determined for each target by elastic scattering of 15-MeV α particles into the spectrometer at a laboratory angle of 20° . Under these conditions, the cross section is expected to be within 0.5% of that for Rutherford scattering. The spectrometer entrance aperture was fixed throughout the experiment. The systematic uncertainty in cross sections determined this way was estimated to be around 5%. Details of the four target foils are given in Table I, where the thicknesses given assume a nominal acceptance of 2.8 msr, determined by previous calibrations using an α source at the target position [21].

TABLE I. Details of the $N = 82$ target foils.

Target	Nominal Thickness $\mu\text{g cm}^{-2}$	Isotopic enrichment %
^{138}Ba	101	99.8(1)
^{140}Ce	144	99.9(1)
^{142}Nd	150	99.0(1)
^{144}Sm	42	93.8(1)

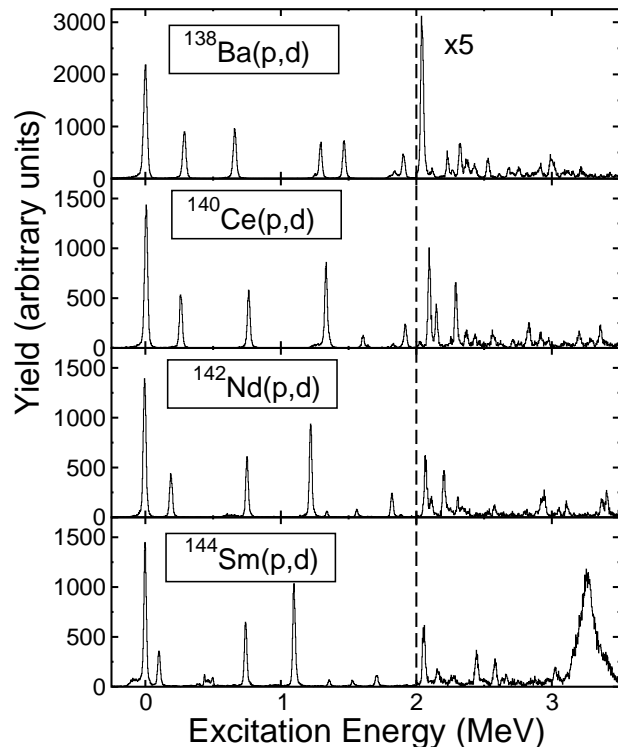


FIG. 2. Deuteron spectra from the (p,d) reaction on targets of ^{138}Ba , ^{140}Ce , ^{142}Nd and ^{144}Sm at an angle of 42° , displayed in terms of the excitation energy of the residual nucleus. The portions of the data to the right of the dotted line have been multiplied by a factor of five for clarity.

Representative focal-plane spectra for each target and reaction are shown in Figures 2 and 3. Comparison of the (p,d) and $(^3\text{He},\alpha)$ data in each case highlight the ℓ sensitivity of the reaction mechanism; for example, the $\ell = 2$ transitions to the $3/2^+$ ground states are visibly stronger in the (p,d) reactions than the $(^3\text{He},\alpha)$ reactions, whose spectra are dominated by the $\ell = 5$ population of an excited $11/2^-$ state at excitation energies ranging from 661 to 754 keV across the residual nuclei. These spectra were calibrated using previously observed states, usefully summarized in References [22–25]. The energy resolution was determined to be ~ 25 keV for (p,d) data and ~ 85 keV for

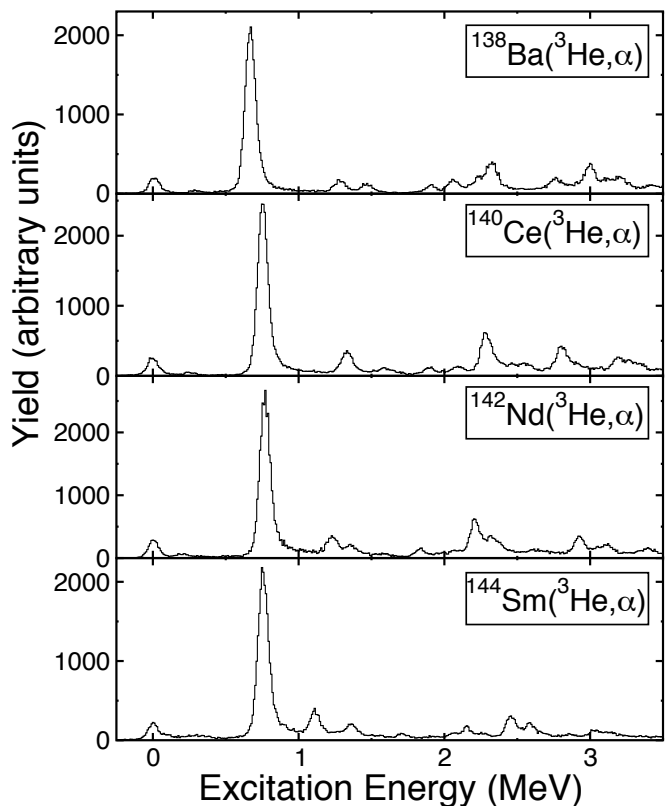


FIG. 3. α -particle spectra from the $(^3\text{He},\alpha)$ reaction on targets of ^{138}Ba , ^{140}Ce , ^{142}Nd and ^{144}Sm at an angle of 15° , displayed in terms of the excitation energy of the residual nucleus.

$(^3\text{He},\alpha)$. Information on the excitation energies of known states, along with a width calibration determined from resolved states, were used to assist the analysis of unresolved peaks, especially in the $(^3\text{He},\alpha)$ spectra. Weak contaminant peaks resulting from the small quantities of ^{13}C and ^{18}O present in the target foils were readily identifiable by their characteristic kinematic shift with angle, which also ensured that states of interest were affected by contaminant contributions at no more than one measurement angle.

Data were collected at laboratory angles of 5° , 20° , 35° and 42° for the (p,d) reaction, chosen to be close to the first maxima of the expected angular distributions for $\ell = 0, 2, 4$ and 5 transitions, respectively. The distributions for the $(^3\text{He},\alpha)$ reaction tend to be less distinct and more forward peaked, so data were only taken at 5° and 15° . An additional angle of 10° was measured for the ^{138}Ba target to assist assignments since the reaction had not been studied previously.

For the majority of the states populated in the residual odd nuclei, angular-momentum quantum numbers have already been determined by a variety of different methods in the literature [22–25]. Previous assignments were checked using the following strategy. The angle of the first maxima of the angular distribution of the (p,d) re-

207 action is generally indicative of the angular momentum
 208 transfer, so the shape of the (p,d) distribution was used in
 209 most cases to determine the ℓ values - some examples of
 210 angular distributions are shown in Figure 4. The angular
 211 distribution for $\ell = 4$ transitions to states in the residual
 212 system were found to be increasingly flat at higher exci-
 213 tation energies, behavior that is reproduced by DWBA
 214 calculations, but still distinct from those of $\ell = 0, 2$
 215 and 5 transitions. (Note that spectroscopic information
 216 for high- ℓ transfer is deduced from the $({}^3\text{He},\alpha)$ reaction
 217 rather than from (p,d) cross sections, as discussed be-
 218 low). To confirm the assignments of high- ℓ transitions,
 219 the slopes of the $({}^3\text{He},\alpha)$ angular distributions, in the
 220 form of the ratio of cross sections at 5° and 15° , were
 221 also used, as illustrated in Fig. 5 for the ${}^{138}\text{Ba}$ target. A
 222 comparison of the two differently-matched reactions has
 223 proved valuable in other work in differentiating between
 224 high- ℓ assignments (some examples can be found in Ref-
 225 erences [7, 9, 26]); it was found to be less useful here in
 226 that respect, but did help to discriminate between high- ℓ
 227 and low- ℓ transitions.

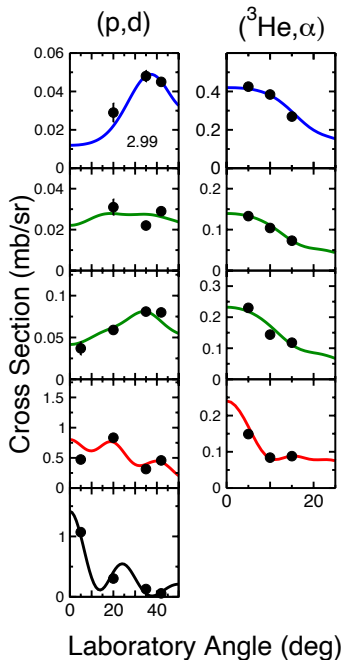


FIG. 4. Examples of angular distributions for the (p,d) and $({}^3\text{He},\alpha)$ reactions compared to the results of DWBA calculations discussed in Section III. The distributions are shown for states populated in ${}^{137}\text{Ba}$ by $\ell = 0$ (black), $\ell = 2$ (red), $\ell = 4$ (green) and $\ell = 5$ (blue) transitions. Transitions with $\ell = 0$ are not strongly populated in the $({}^3\text{He},\alpha)$ reaction. The angular distributions are labeled with the excitation energy in the residual system in units of MeV.

228 The ℓ values deduced from the current work for the
 229 three heaviest targets are generally consistent with the
 230 work on (d,t) and $({}^3\text{He},\alpha)$ reactions by Berrier *et al.* [14].
 231 There is very good agreement for ${}^{141}\text{Nd}$. We note only
 232 minor discrepancies with Ref. [14] in ${}^{139}\text{Ce}$; strength at

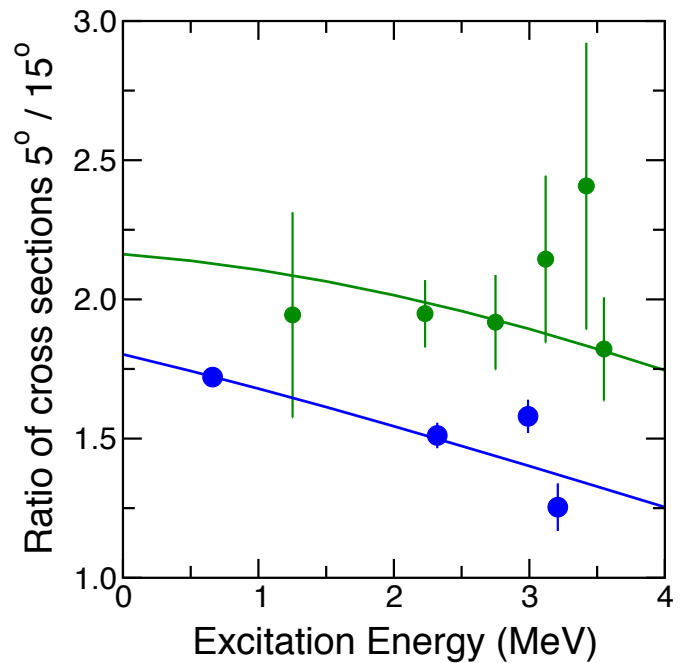


FIG. 5. An example of the ratio of cross section at 5° and to that at 15° for the $({}^3\text{He},\alpha)$ reaction, here shown for the population of states in ${}^{137}\text{Ba}$ for $\ell = 4$ (green) and $\ell = 5$ (blue) as a function of excitation energy. The solid lines are the results of DWBA calculations discussed in Section III.

233 2.910 and 3.352 MeV had previously each been found to
 234 carry *both* $\ell = 2$ and 4, but here no evidence for the pres-
 235 ence of $\ell = 4$ is found in the former and conversely, no evi-
 236 dence for $\ell = 2$ in the latter. The population of the state
 237 at 2.018 MeV has been noted by several authors to have a
 238 non-standard distribution in neutron-removal reactions,
 239 which is confirmed here and no firm assignment could be
 240 made. The current work finds evidence for the presence
 241 of a tentative $\ell = 0$ contribution at 2.556 MeV, along
 242 with the stronger $\ell = 4$ transition. Spectroscopic factors
 243 for this doublet were determined on the basis that the
 244 (p,d) cross section at forward angles is due to the $\ell = 0$
 245 strength and that this component does not contribute to
 246 the $({}^3\text{He},\alpha)$ cross section, which was attributed entirely
 247 to $\ell = 4$.

248 Assignments in ${}^{143}\text{Sm}$ also agree well with Ref. [14].
 249 However, at a beam energy of 23 MeV, elastically-
 250 scattered protons have a lower kinetic energy and mag-
 251 netic rigidity than deuterons arising from the popula-
 252 tion of the ground-state groups in the (p,d) reaction.
 253 Whilst the proton groups are fairly well separated from
 254 deuterons by energy-loss characteristics, a proton tail
 255 does contaminate the deuteron gating conditions, espe-
 256 cially at larger angles. This is the origin of the broad peak
 257 above 3 MeV in the ${}^{144}\text{Sm}(p,d)$ reaction in Figure 2. Simi-
 258 lar groups in data on other targets lie higher in effective
 259 excitation energy than was studied here. Previous work
 260 has been performed at higher energies [15], moving the
 261 elastic group to higher effective excitation energies, which

circumvented this issue. The $(^3\text{He},\alpha)$ reaction does not suffer the same problem with elastic scattering, but without the (p,d) data, assignments are more difficult. The two states at 3.13 and 3.23 MeV observed in the current work with the $(^3\text{He},\alpha)$ reaction are likely to be populated via high- ℓ transitions, but differentiation between $\ell = 4$ and 5 has not been possible. For the later discussion, unobserved $\ell = 5$ transitions would be a more critical issue; Ref. [14] observes no further $\ell = 5$ population, whereas Ref. [15] isolates two higher-lying $\ell = 5$ transitions. If the states at 3.13 and 3.23 MeV were $\ell = 5$, it would shift the centroid of that strength in ^{143}Sm by around 100 keV, which would not significantly alter the interpretation presented below.

In ^{137}Ba , assignments up to 2 MeV are in agreement with those of previous (p,d) reactions [12, 13]. The $7/2^+$ peak at 1.252 MeV in the current work, also observed by several other techniques [22], has a J^π assignment from γ -decay measurements following Coulomb excitation [27]. It was missed in both previous (p,d) experiments, presumably masked by its more intense $\ell = 2$ neighbour at 1.290 MeV. Ref. [12] also identified tentative assignments of the $7/2^+$ state at 2.230 MeV and the $11/2^-$ state at 2.320 MeV, which are confirmed here and supported by the $(^3\text{He},\alpha)$ data for the first time. The $\ell = 4$ transitions also found in that work at 2.54 and 2.99 MeV have been revised here as $\ell = 2$ and $\ell = 5$, respectively. The former state is not observed strongly in the $(^3\text{He},\alpha)$ reaction, so the $\ell = 4$ assignment of Ref. [12] is not confirmed. The latter state has angular distributions in both reactions that are more consistent with $\ell = 5$. The previous $\ell = 4$ assignment in Ref. [12] may have been affected by the state at 3.03 MeV, which was unresolved from that at 2.99 MeV; the states were resolved, but no assignment was made, in Ref. [13]. In addition, 11 new assignments in ^{137}Ba are made here, mainly $\ell = 2$ states at excitation energies above 2.3 MeV.

The energies and ℓ assignments of all states observed are summarized in Table II, along with spectroscopic factors determined using the procedures outlined below. Detailed data on cross sections are available as Supplemental Information [28]. The J^π values listed in this table are taken from other measurements [22–25]; where J^π assignments are not available, the subsequent analysis takes a model-dependent assumption that the strength is from the valence shell. However, in many cases, there is insufficient information to properly assign spin-parity to $\ell = 2$ strength.

Although the extraction of single-particle strength using DWBA calculations is not discussed until the following section, it is useful at this point to consider the general picture of the strength distributions in the residual nuclei, which is illustrated in Figure 6; the comparison with particle-vibration coupling calculations will be discussed later. The general pattern of behavior is similar to that revealed in neutron-removal reactions on $^{134,136}\text{Ba}$ [29] and $^{128,130}\text{Te}$ [30]. The ground state in each case is a $3/2^+$ state carrying a significant fraction of the ex-

pected $d_{3/2}$ strength, increasing with Z from around 64% in ^{137}Ba to 85% in ^{143}Sm . Older studies have made the assumption that this state carries all of the $d_{3/2}$ strength [11–13]. At a few 100 keV in excitation energy, there is a $1/2^+$ state with significant $s_{1/2}$ strength (90% on average and not varying significantly across the isotopes). Beyond that lies a strong $11/2^-$ state with around 80% of the expected $h_{11/2}$ strength. These correspond to the three low-lying strong peaks that can be seen in the (p,d) spectra (see Fig. 2) and the population of the $11/2^-$ state dominates the $(^3\text{He},\alpha)$ spectra (see Fig. 3). At higher excitation energies, there is a second strong $\ell = 2$ transition above 1 MeV, obvious in the (p,d) reactions on ^{140}Ce , ^{142}Nd and ^{144}Sm targets, which has been given a $5/2^+$ assignment in other work, carrying between 35 and 50% of the $d_{5/2}$ strength. In ^{137}Ba , the corresponding state has a lower strength and an additional, relatively strong $3/2^+$ state occurs just above in excitation energy.

Above ~ 1.8 MeV in each residual nucleus, there are numerous small fragments of strength, which appear to be dominated by $\ell = 2$ and $\ell = 4$ strength, with a few even weaker isolated $\ell = 0$ and $\ell = 5$ transitions. It therefore appears that most of the strength associated with the $s_{1/2}$, $d_{3/2}$ and $h_{11/2}$ orbitals are generally contained in a low-lying state with low levels of fragmentation. The low-lying $\ell = 4$ state apparent around 1.2 MeV in Sm, Nd and Ce final nuclei only carries only around 10% of the $g_{7/2}$ strength, the rest is dispersed in small fragments at high excitation energies with a significant proportion lying at higher excitation energies than studied here; this 10% fragment does not appear in ^{137}Ba . Across all the residual nuclei the deeper-lying $d_{5/2}$ and $g_{7/2}$ hole strengths are significantly fragmented over many states extending to high excitation energies.

III. DWBA AND NORMALIZATION

Spectroscopic factors were determined from the measured cross sections by comparison with the results of calculations using the distorted-wave Born approximation with the finite-range code PTOLEMY [31]. The approach taken here is same procedure adopted in a recent global analysis of quenching of spectroscopic strength [43], which has also been used in a number of recent studies, for example Refs. [26, 32, 49]. The choices for potentials associated with the optical models describing the initial and final reaction channels, and those associated with the neutron bound states in the light and heavy cores, are the same as those used previously, with one minor exception, and are summarized below.

The incoming and outgoing partial waves were described using the global optical potentials for protons [35], deuterons [36], and helions [37]. The deuteron potential used here gave a better reproduction of the angular distributions than more recent global potentials [38] that we have employed in previous cases. The potential of Ref. [36] had been used as the starting point in

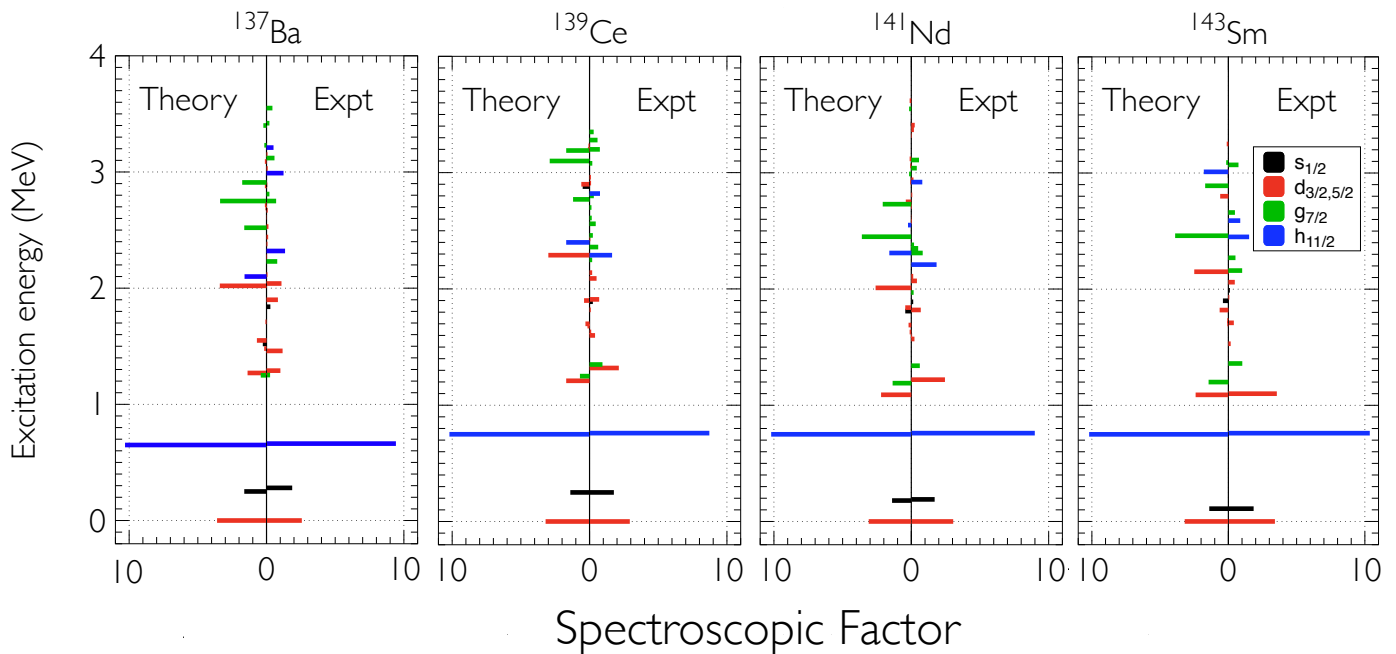


FIG. 6. Distribution of spectroscopic strength of states populated in (p,d) and $({}^3\text{He},\alpha)$ reactions for $\ell = 0$ (black), $\ell = 2$ (red), $\ell = 4$ (green) and $\ell = 5$ (blue) transitions as a function of the excitation energy in the residual systems, compared to particle-vibration coupling calculations from Ref. [10]. The strength of individual states has been obtained from measured reaction cross sections using procedures described in Section III.

375 the search for new parameters to extend the potential to
 376 wider energy range in Ref. [38], but the current deuteron
 377 energies are within those used in the former potential. A
 378 fixed α -particle potential determined from the $A = 90$
 379 region was used [39].

380 Recent microscopic calculations were used as the
 381 source for the internal wave functions of the light ions in
 382 the reactions. For the deuteron, form factors determined
 383 using the Argonne v_{18} potential were used [33] and those
 384 for the α particle and ${}^3\text{He}$ ions were taken from recent
 385 Green's function Monte-Carlo calculations [34].

386 The wave functions of the transferred neutron in the
 387 heavy bound state were generated using a Woods-Saxon
 388 potential with a depth adjusted to match the measured
 389 binding energy. This used fixed geometric parameters:
 390 radius parameter $r_0=1.28$ fm and diffuseness $a = 0.65$ fm.
 391 The derivative of a Woods-Saxon potential with radi-
 392 us $r_{so}=1.10$ fm, diffuseness $a_{so} = 0.65$ fm and depth
 393 $V_{so}=6$ MeV was used to model the spin-orbit component.

394 The approximations involved in the DWBA approach
 395 are best satisfied where there is a large probability of a di-
 396 rect reaction mechanism. Spectroscopic factors are there-
 397 fore extracted using experimental cross sections mea-
 398 sured as close as possible to the angle of the first maxi-
 399 mum of the angular distribution of the most appropri-
 400 ately matched reaction. The (p,d) reaction was used to
 401 determine the spectroscopic strength for $\ell = 0$ and 2 from
 402 data at 5° and 20° , respectively, whereas that for $\ell = 4$
 403 and 5 was extracted from the $({}^3\text{He},\alpha)$ reaction at 5° .

404 The DWBA calculations carry an overall uncertainty

405 in absolute normalization. Consistent results have been
 406 obtained by adopting systematic approaches (for exam-
 407 ple, Ref. [8, 9]) using the Macfarlane-French sum rules
 408 [40] which associate the summed spectroscopic strengths
 409 to the occupancies and vacancies of single-nucleon or-
 410 bitals. If a normalization factor is chosen such that the
 411 total observed strength is equal to the full single-particle
 412 value, the degree to which that factor deviates from unity
 413 is related to quenching of single-particle strength. Such
 414 quenching has been observed in other reactions, such
 415 as $(e,e'p)$ [41, 42], where the total low-lying strength
 416 accounts for approximately half that expected by the
 417 independent-particle model. A recent large-scale analysis
 418 of transfer data has found normalization factors that are
 419 quantitatively consistent with previous studies of such
 420 quenching [43] and here we follow the same procedure.

421 The total spectroscopic strength was required to repro-
 422 duce the number of expected neutrons in the correspond-
 423 ing orbital in the target nucleus. On the assumption of
 424 the closed neutron shell at $N = 82$, this corresponds to
 425 the degeneracy of the orbital. This assumption can be
 426 tested by probing the vacancy of the orbitals below the
 427 shell closure by looking for population of the relevant
 428 ℓ transfer in (d,p) reactions on $N = 82$ targets. Sev-
 429 eral such studies exist in the literature, but evidence for
 430 population of orbitals with the quantum numbers of the
 431 nominally-filled neutron orbitals is sparse and any such
 432 states are populated very weakly. As examples, Ref. [44]
 433 observes an $\ell = 0$ transition at 3.351 MeV and three ten-
 434 tative $\ell = 2$ transitions above 2.2 MeV, with strengths of

TABLE II. Summary of states populated in neutron-removal reactions on $N = 82$ targets, including excitation energy E , orbital angular momentum transfer ℓ , spin-parity J^π , and normalised spectroscopic factor C^2S . Excitation energies are given in MeV and are estimated to carry an uncertainty of ~ 5 keV, rising to ~ 10 keV in the case of ^{137}Ba at higher excitation energies. The spectroscopic factors are deduced from the (p,d) reaction for $\ell = 0$ and 2 transfers and from the $(^3\text{He},\alpha)$ reaction for $\ell = 4$ and 5, and have been normalized using the method described in the text. The errors in the normalised values are typically 5% due to variation of DWBA with different input parameters, but for weaker transitions these rise where statistical errors become more significant (more information is available in the Supplemental Material [28]). J^π are taken from the literature [22–25]; where a J^π value is not listed, a model-dependent assumption was made that the single-particle orbitals is in the valence shell.

^{137}Ba				^{139}Ce				^{141}Nd				^{143}Sm			
E	ℓ	J^π	C^2S	E	ℓ	J^π	C^2S	E	ℓ	J^π	C^2S	E	ℓ	J^π	C^2S
0.000	2	$3/2^+$	2.56	0.000	2	$3/2^+$	2.92	0.000	2	$3/2^+$	3.04	0.000	2	$3/2^+$	3.40
0.281	0	$1/2^+$	1.86	0.252	0	$1/2^+$	1.77	0.192	0	$1/2^+$	1.69	0.110	0	$1/2^+$	1.84
0.662	5	$11/2^-$	9.42	0.755	5	$11/2^-$	8.72	0.759	5	$11/2^-$	8.99	0.758	5	$11/2^-$	10.36
1.252	4	$7/2^+$	0.26	1.321	2	$5/2^+$	2.12	1.222	2	$5/2^+$	2.44	1.100	2	$5/2^+$	3.54
1.290	2	$5/2^+$	1.01	1.347	4	$7/2^+$	0.94	1.343	4	$7/2^+$	0.62	1.362	4	$7/2^+$	1.02
1.460	2	$3/2^+$	1.17	1.598	2	$(3/2)^+$	0.40	1.565	2	$(3/2)^+$	0.23	1.533	2	$(5/2)^+$	0.17
1.840	0	$1/2^+$	0.28	1.632	2	$3/2^+$	0.12	1.597	2	$(3/2,5/2)^+$	0.06	1.708	2	$(3/2)^+$	0.40
1.900	2	$3/2^+$	0.83	1.823	2	$5/2^+$	0.09	1.822	2	$5/2^+$	0.69	1.930	2	$5/2^+$	0.07
2.040	2	$(5/2)^+$	1.08	1.889	0	$1/2^+$	0.24	1.888	0	$1/2^+$	0.14	1.990	0	$1/2^+$	0.11
2.117	2		0.07	1.911	2	$(3/2)^+$	0.69	1.968	4	$7/2^+$	0.17	2.064	2	$7/2^+$	0.47
2.230	4	$7/2^+$	0.78	2.018				2.070	2	$(3/2^+,5/2^+)$	0.41	2.161	4	$7/2^+$	1.01
2.271	2		0.04	2.090	2		0.51	2.111	2	$3/2^+,5/2^+$	0.14	2.274	4	$7/2^+$	0.52
2.32	5	$(3/2^+,5/2)$	1.35	2.143	2		0.19	2.180	0		0.05	2.450	5		1.52
2.38	2		0.07	2.251	(4)	$(7/2^+)$	0.19	2.208	5	$(11/2)^-$	1.84	2.586	5		0.87
2.44	2		0.12	2.286	5	$11/2^-$	1.63	2.31	4	$7/2^+, (9/2^+)$	0.83	2.662	4		0.48
2.53	2		0.14	2.362	4		0.63	2.349	4		0.50	3.05	(4)		0.64
2.61	(2)		0.02	2.426	2		0.06	2.384	4		0.20	3.13			
2.67	2		0.09	2.455	(4)		0.24	2.512	4		0.05	3.23			
2.75	4		0.70	2.556	4 & (0)		0.45 & 0.04	2.581	(2)		0.05				
2.81	(4)		0.21	2.610	(4)		0.16	2.616	(2)		0.02				
2.89	2		0.06	2.701	(4)		0.14	2.705	(2)		0.05				
2.99	5		1.24	2.800	4	$7/2^+$	0.31	2.809	(2)		0.07				
3.03	2		0.09	2.822	5	$9/2^-, 11/2^-$	0.76	2.915	5		0.80				
3.12	4		0.58	2.910	2		0.11	2.939	2		0.16				
3.15	(2)		0.07	2.964	2		0.10	3.042	4		0.40				
3.21	5		0.51	3.082	(4)		0.20	3.112	4		0.56				
3.42	4		0.21	3.196	4		0.75	3.315	(2)		0.04				
3.55	4		0.43	3.282	4		0.58	3.369	2		0.19				
				3.352	4		0.30	3.407	2		0.25				

435 around 1% in ^{141}Ce . Ref. [45] reports an $\ell = 0$ transition
 436 at 1.616 MeV in ^{143}Nd with a similar intensity. Such
 437 weak transitions are also likely to be subject to higher
 438 contributions from indirect processes. There appears to
 439 be no evidence for the relevant ℓ transfer in ^{139}Ba or
 440 ^{145}Sm . The assumption of a closed shell looks reason-
 441 able, at least compared to other uncertainties.

442 Initially normalization was performed separately for
 443 each ℓ value in the appropriately matched reaction and
 444 the results are shown in in Table III.

TABLE III. Normalization factors for DWBA calculations with the associated mean and standard deviation across the four targets studied. Asterisks indicate cases that are affected by significant unobserved strength.

	(p, d)		$(^3\text{He}, \alpha)$	
	$\ell = 0$	$\ell = 2^*$	$\ell = 4^*$	$\ell = 5$
^{138}Ba	0.58	0.40	0.22	0.58
^{140}Ce	0.55	0.40	0.40	0.52
^{142}Nd	0.51	0.42	0.23	0.54
^{144}Sm	0.53	0.44	0.31	0.59
Mean	0.54	0.41	0.27	0.56
St Dev	0.03	0.02	0.06	0.04

445 The mean normalization factors for the $\ell = 0$ and $\ell = 5$
 446 are 0.54 and 0.56, respectively, with a variation of around
 447 0.03 across the targets. These values compare favourably
 448 with a recent systematic analysis of transfer data on tar-
 449 gets from ^{16}O to ^{208}Pb for a variety of different proton
 450 and neutron transfer reactions over a range of ℓ values,
 451 which deduced a quenching with respect to independent-
 452 particle models of 0.55 [43]. The mean quenching factors
 453 deduced in that work for low ℓ transitions in (d, p) and
 454 (p, d) reactions was 0.53; the excellent correspondence
 455 with the current normalization for $\ell = 0$ is particularly
 456 encouraging. It relieves a potential concern that, given
 457 measurements at 0° are not possible, $\ell = 0$ spectroscopic
 458 factors cannot be obtained as close to the first maxi-
 459 mum of the angular distribution as other ℓ values and,
 460 by necessity, are extracted in a region of a rather strongly
 461 sloping angular distribution.

462 However, the average values for $\ell = 2$ and $\ell = 4$, at
 463 0.41 and 0.27, respectively, are significantly lower. This
 464 suggests that the experiment is missing some of the low-
 465 lying strength associated with the corresponding orbitals.
 466 This finding is not inconsistent with the observed distri-
 467 bution of high-lying, dispersed and fragmented strength
 468 for $\ell = 2$ and 4 (see Fig. 6) where the risk of missing
 469 strength is high, either in the form of transitions lying
 470 outside the measured excitation range or in the form of
 471 small unresolved fragments of strength in the measured
 472 spectra. We therefore adopt the values of 0.54 and 0.56
 473 for the DWBA normalizations for the (p, d) and $(^3\text{He}, \alpha)$
 474 reactions, respectively.

475 The choice of potentials used in the DWBA calcula-
 476 tion has a significant effect on the absolute magnitude of

477 the raw unnormalised spectroscopic factors; calculations
 478 were repeated with a number of other physically reason-
 479 able potentials and a variation of $\sim 20\%$ in the calculated
 480 absolute cross sections was found. *Normalised* spectro-
 481 scopic factors, determined using the procedures outlined
 482 above, are far less sensitive to choices of optical models
 483 and were found to vary by around $\sim 5\%$. The influence of
 484 multi-step processes is expected to be similar to that es-
 485 timated in other analyses [9, 26] and are a less significant
 486 effect.

487 There is a small complication that arises for neutron-
 488 removal (and proton-adding) reactions associated with
 489 isospin effects. In these reactions, the transfer results
 490 in the population of states with both isospin couplings,
 491 $T \pm 1/2$ where T is the target isospin. The states corre-
 492 sponding to the higher isospin coupling $T_>$ lie at excita-
 493 tion energies higher than those accessed here experimen-
 494 tally. In principle, the Macfarlane and French sum rules
 495 used in the normalization procedure for neutron-removal
 496 reactions need to include the $T_>$ strength. This can be
 497 done on the basis of isospin symmetry, using spectro-
 498 scopic factors C^2S for analogous states in proton-removal
 499 reactions and applying the appropriate isospin Clebsch-
 500 Gordan coefficients to deduce the spectroscopic factor as-
 501 sociated with the higher isospin [46].

502 The nuclei studied here are near the beginning of the
 503 $Z = 50-82$ shell and protons are known to occupy mainly
 504 the $g_{7/2}$ and $d_{5/2}$ orbitals [47]; the spectroscopic factors
 505 for proton removal from the $\ell = 0$ and 5 orbitals relevant
 506 for the normalisation are consequently small (see Fig-
 507 ure 7). Moreover, the ratios of isospin Clebsch-Gordan
 508 coefficients that are required to convert these into the
 509 spectroscopic factors for the higher isospin states in neu-
 510 tron removal are also small. The overall correction for the
 511 non-observation of the upper isospin component is less
 512 than a 1% effect for these orbitals and is smaller than
 513 other uncertainties. The correction has therefore been
 514 neglected in the normalization procedure here. Larger
 515 corrections would apply to the summed strengths for $g_{7/2}$
 516 and $d_{5/2}$, which have significant population of protons
 517 and large proton removal strengths, but these are not
 518 used to determine the normalization.

519 IV. DISCUSSION

520 Spectroscopic factors, extracted using the procedure
 521 outlined in the previous section, were used to determine
 522 the centroids of observed single-neutron hole strengths
 523 for the $T_<$ isospin components. These centroids and the
 524 associated summed strength are summarized in Table IV
 525 and shown as a function of atomic number in Figure 8.

526 In some previous studies, it has been assumed that
 527 the $3/2^+$ ground state exhausted the $d_{3/2}$ strength, but
 528 here it is found that the associated spectroscopic fac-
 529 tor increases from ^{137}Ba to ^{143}Sm . In addition to the
 530 total $\ell = 2$ strength, Table IV also shows values asso-
 531 ciated with $\ell = 2$ transitions populating states with a

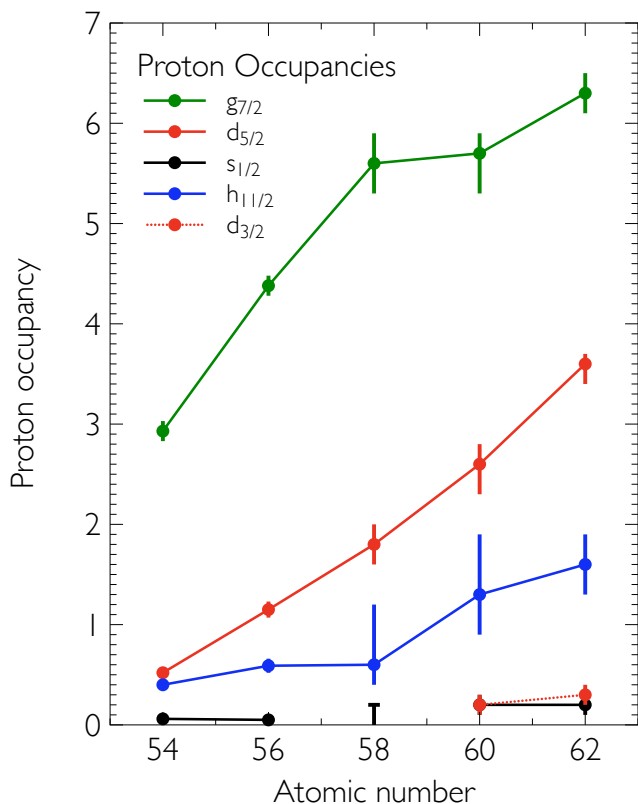


FIG. 7. Occupancy of single-proton orbitals in $N = 82$ nuclei as a function of proton number, taken from Ref. [47] for Ce, Nd and Sm and Ref. [49] for Xe and Ba. No proton strength was observed for the $s_{1/2}$ orbital in Ref. [47] for Ce and an upper limit of 0.2 was placed on the associated occupancy.

firm or tentative $3/2^+$ spin assignment and the centroid of these are shown in Fig. 8. The associated summed strengths are not as consistent across the isotopes as for the other ℓ values, indicating that in some cases there is missing $d_{3/2}$ strength and in others that there are likely some mis-assignments of j values. The remaining $\ell = 2$ strength is likely attributable to the $d_{5/2}$ orbital, but it varies between 50% and 76% of the full strength across the isotopes. Fragmentation is high and a significant portion of the strength lies at excitation energies higher than measured here.

In the case of the $g_{7/2}$ strength, there is significant missing strength and the current work only observed between 40 and 61%, depending on the isotope. The true single-particle centroid lies higher than the observed centroid quoted in Table IV; we estimate that the true centroid lies at least 450, 350, 700 and 600 keV higher in energy than the observed centroids in ^{137}Ba , ^{139}Ce , ^{141}Nd and ^{143}Sm , respectively, and because of this large uncertainty, we make no further discussion of $\ell = 4$ strength here.

In the cases where most of the low-lying strength has been captured ($\ell = 0$ and 5), the centroid across both $T_<$

and $T_>$ isospin components would reflect the underlying single-neutron energy. As discussed above, only the $T_<$ strength is observed in the current work. The location and strength of the $T_>$ component were estimated using Coulomb displacement energies and data from proton-removal reactions [47] using isospin symmetry. It was found that the difference between the full centroid and that for the $T_<$ component of the $\ell = 0$ and 5 strength increases with Z from around 20 to 90 keV across the isotopes. This is relatively small since the associated orbitals have low proton occupancy. The correction is much larger for $\ell = 2$ and 4 strength, but these are the same orbitals where significant strength remains unobserved in the current experiment and the interpretation of the measured centroids is difficult. We therefore use the variation in the measured centroids of $\ell = 0$ and 5 strength as an estimate for the changes in the underlying single-neutron energies across the isotones studied.

Changes in orbital energies across chains of nuclides have been interpreted in terms of the effect of valence proton-neutron interactions as the nucleon number varies. Here we follow the approach of Reference [2] where changes in the effective single-neutron energies were compared to calculations using a two-body central plus tensor force between neutrons and valence protons, taking information on proton occupancy from proton-transfer experiments in the literature.

The occupancies of single-proton orbitals are available from previous measurements of proton removal using the ($d, ^3\text{He}$) reaction. Reference [47], which reports reactions on $N = 82$ nuclei from Xe through to Sm, is broadly in agreement with a contemporaneous study on Ba, Ce and Nd [48]. A more recent study has been made of Xe and Ba nuclei [49] with higher precision. Here we adopt the ^{138}Ba occupancies from Ref. [49] and those for ^{140}Ce , ^{142}Nd and ^{144}Sm from Ref. [47].

The pattern of proton occupancies is illustrated in Figure 7, showing significant occupation of the $g_{7/2}$ and $d_{5/2}$ orbitals. The occupancy of the $g_{7/2}$ orbital increases until $Z = 58$, beyond which the changes in occupancy are mainly in the $d_{5/2}$ orbital. Other orbitals are filled to less than 10%. The $h_{11/2}$ orbital gradually increases in population across the isotopes, but remains small. Evidence for a low level of occupancy of the $s_{1/2}$ orbital by protons has been found in all nuclei, except for ^{140}Ce where only an upper limit is available. The proton occupancy of the $d_{3/2}$ orbital begins to be observable in the two heaviest systems. Although the population of low- ℓ single-proton states are small, they can have a significant effect on the energies of certain neutrons where the orbital overlap is large.

Calculations of the changes in effective single-neutron energies presented here were performed using the effective two-body force from Reference [53] (labelled here as HKT) which was deduced from a G-matrix treatment of the Paris nucleon-nucleon interaction. The results obtained with that force are very similar to those done using the phenomenological Schiffer and True [50] interaction.

TABLE IV. Observed summed hole strengths and the associated centroid excitation energies for the $T_<$ components. The summed strength is deduced from spectroscopic factors that were normalized using the method described in the text. The errors quoted on the summed strength are on the basis of the variations due to choices of potentials in the DWBA (see text for details). The errors on the centroid in the table are statistical. Values are given for the sum of $d_{3/2}$ and $d_{5/2}$ orbitals deduced for the $\ell = 2$ transitions and also separately for states populated by $\ell = 2$ transitions with a spin-3/2 assignment in the literature. Asterisks indicate cases that are affected by significant unobserved strength, which gives rise to a significant systematic uncertainty in the true single-particle centroid.

Orbital	Summed Strength				Expected	Centroid Energy (MeV)			
	^{137}Ba	^{139}Ce	^{141}Nd	^{143}Sm		^{137}Ba	^{139}Ce	^{141}Nd	^{143}Sm
$s_{1/2}$	2.1(1)	2.0(1)	1.87(9)	1.9(1)	2	0.48(1)	0.48(2)	0.37(1)	0.21(1)
d^*	7.4(4)	7.3(4)	7.8(4)	8.0(4)	10	1.19(2)	1.01(2)	1.07(3)	0.74(3)
$d_{3/2}$	4.6(2)	4.1(2)	3.26(16)	3.8(2)	4	0.72(2)	0.52(2)	0.11(2)	0.18(2)
$g_{7/2}^*$	3.2(2)	4.9(2)	3.27(16)	4.4(2)	8	2.73(2)	2.56(3)	2.32(2)	2.20(3)
$h_{11/2}$	12.5(6)	11.1(6)	11.6(5)	12.7(6)	12	1.17(2)	1.12(2)	1.14(2)	1.08(2)

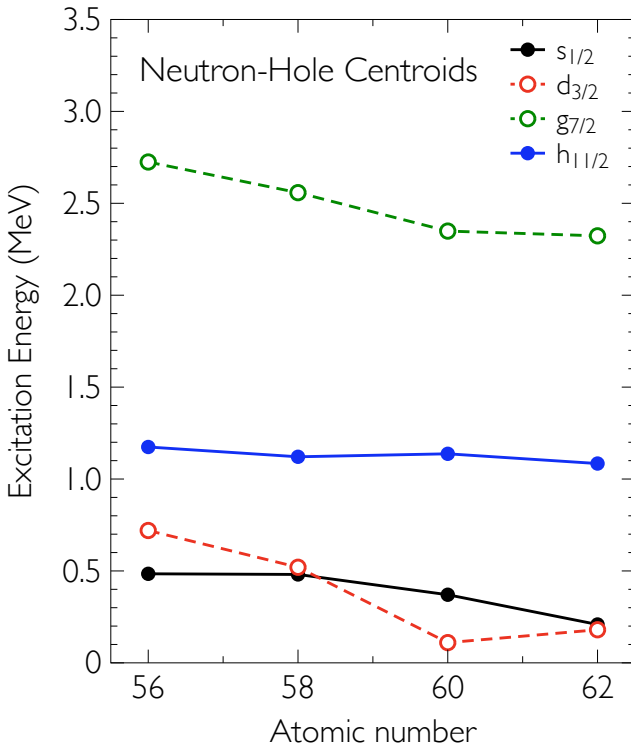


FIG. 8. Variation in the excitation energy of the centroid of *observed* single-particle strength for the $T_<$ component as a function of proton number. Statistical errors are of the order ~ 10 keV. The open circles and dotted lines indicate instances where the full single-particle strength has not been observed. The centroid for the $d_{3/2}$ orbital uses states that have a $3/2^+$ spin-parity in the literature. The data for the $g_{7/2}$ orbital suffers from significant unobserved strength outside of the excitation-energy range measured and the true single-particle centroid will lie significantly higher than the observed centroid (see text for details).

Both used single-particle wave functions from infinite oscillator potentials. Individual matrix elements were calculated using the computer code of Reference [54],

proton-neutron monopole shifts were constructed (these are available as part of the Supplemental Information [28]) and the changes in neutron single-particle energy across the $N = 81$ nuclei were obtained using the proton occupancies described above.

To study the effect of the proton occupancy on the relative changes in neutron binding as a function of proton number across the isotopes studied, the experimental data (solid dots) are plotted in Figure 9. A smooth increase in the binding energy of the neutron $s_{1/2}$ and $h_{11/2}$ orbitals is found when adding protons, due to the trends in proton occupancy shown in Figure 7, and the fact that many of the monopole terms have a similar amplitude. Consequently, the effective energy follows that of an averaged global trend of an attractive proton-neutron interaction. Since some of the two-body interactions are different, the change in binding was calculated using the monopole shifts with the HKT interaction and the experimental proton occupancies. Since only the variation with A is meaningful, the absolute value of these calculations along the vertical axis in the figure was shifted to fit the experimental points. These calculations, including the experimental uncertainties in the proton occupancies, are represented by the shaded areas. (Additionally, the two-body matrix elements themselves are subject to some uncertainty. This is rather difficult to estimate, but is likely of the order of 10%).

The monopole shifts for neutron states are particularly sensitive to uncertainties in the occupancy of the corresponding proton orbital due to their large overlap. This is compounded in the case of Ce where only an upper limit on the $s_{1/2}$ proton occupancy had been determined. Indeed, the case of $s_{1/2}$ may be more complicated if some of the weak unassigned strength in the proton-removal reactions is in reality $\ell = 0$; for example, there is unassigned strength in the $^{136}\text{Ba}(d,^3\text{He})$ reaction that amounts to around 0.1 protons (see Table VIII in Ref. [49]).

The trend in the energy of the neutron $h_{11/2}$ orbital appears reasonably well reproduced by the calculations, as shown in Figure 9, but the slope of the neutron $s_{1/2}$ orbital is less well predicted in the calculations using

657 monopole shifts from the HKT interaction with harmonic
 658 oscillator wave functions. The difference in slope in Fig-
 659 ure 9 between the data and the monopole-shift calcu-
 660 lations for the neutron $s_{1/2}$ orbital suggests that other
 661 effects are playing a role for that single-particle state.

662 The two-body matrix elements yielding the monopole
 663 shifts were calculated using single-particle wave functions
 664 in an infinite harmonic oscillator potential where the order-
 665 ing of the different states is fixed. However, any poten-
 666 tial with finite binding is subject to geometric effects
 667 such that the single-particle states behave somewhat dif-
 668 ferently depending on their binding energy relative to the
 669 height of the binding potential including the centrifugal
 670 term (and Coulomb effects where relevant). Such effects
 671 are known; for instance, they were demonstrated in Fig
 672 2.30 of Ref. [51] where different neutron orbitals in the
 673 50-82 shell have different behaviors as a function of A ,
 674 notably the $s_{1/2}$ state, and this was discussed in more
 675 detail in Ref. [52].

676 The mean field is a sum of two-body interactions, but
 677 it is not easy to separate effects that depend on angular
 678 momentum (such as the tensor interaction) from those
 679 caused by geometric effects from finite binding. It is
 680 therefore instructive to also compare the data to Woods-
 681 Saxon calculations, where geometric effects are included,
 682 but the angular-momentum dependence from the two-
 683 body interaction is not. Fig. 9 shows the results of such
 684 calculations with standard radius and asymmetry terms,
 685 with parameters fixed to the binding energy of the $11/2^-$
 686 state in ^{137}Ba . Such calculations do appear to better re-
 687 produce the slope of the $s_{1/2}$ data.

688 Given these limitations, the level of agreement between
 689 data and monopole-shift calculations displayed in Fig. 9
 690 is probably reasonable, and constitutes a check on how
 691 well the changes in binding energies across the isotopes
 692 can be reproduced by the effect of microscopic interac-
 693 tions.

694 The interpretation of experimental centroids in terms
 695 of monopole-shift calculations presented above is a coarse
 696 comparison and it would be useful to understand the frag-
 697 mentation of single-neutron hole strength across states in
 698 the populated nucleus. The general distribution of trans-
 699 fer strength revealed here is reasonably well reproduced
 700 by particle-vibration coupling calculations performed a
 701 number of years ago [10], given the limitations of the
 702 model used (see Fig. 6). The strong low-lying $\ell = 0, 2$
 703 and 5 strength is well reproduced and, although the level
 704 of fragmentation is lower than observed due to the res-
 705 trictions in the model space used, smaller fragments of
 706 strength are predicted at higher excitations. The $\ell = 4$
 707 strength is predicted to be higher-lying and fragmented,
 708 as observed, but any state-to-state correspondence be-
 709 tween the experimental data and calculated strength is
 710 difficult due to the extent of the fragmentation seen in
 711 the experiment.

712 It would be interesting to compare the strength distri-
 713 butions with the results from modern large-scale shell-
 714 model calculations. However, the dimensions of the

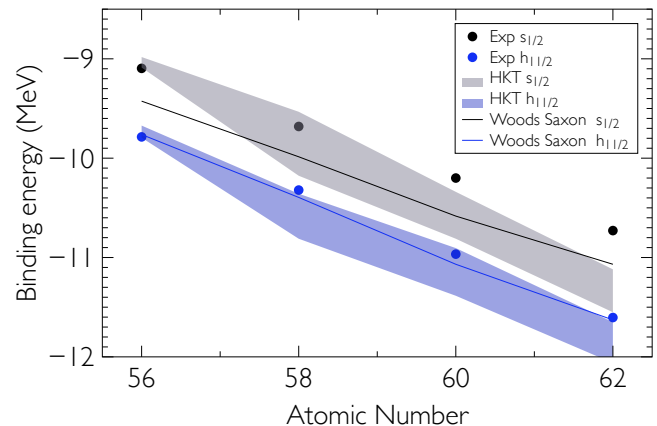


FIG. 9. Experimental single-particle binding energies for the neutron $s_{1/2}$ (black) and $h_{11/2}$ (blue) orbitals, deduced from the centroids of hole excitation energies. Calculations used the effective two-body interaction (HKT) of Ref. [53] and proton valence occupancies from Refs. [47, 49]. These are shown as bands reflecting the uncertainties in the proton occupancies and the absolute value of these calculations along the vertical axis in the figure was shifted to fit the experimental points (see text for more details). The solid lines are Woods-Saxon calculations with standard radius and asymmetry terms with parameters fitted to the $11/2^-$ state in Ba.

715 model space in such a large shell are currently rather
 716 difficult to manipulate, making such calculations tricky.
 717 Some shell-model calculations have been made around
 718 $A = 130$ nuclei [55], which includes ^{137}Ba as one of the
 719 heaviest systems considered. Pair-truncated shell-model
 720 calculations have been discussed for ^{137}Ba and ^{139}Ce [56].
 721 The results in both cases have so far only been compared
 722 to level energies and electromagnetic moments; predic-
 723 tions of spectroscopic factors are not readily available in
 724 the literature. We hope that the current data will inform
 725 large-scale calculations as they become available in the
 726 future.

727 In summary, neutron-hole strength in the $N = 81$ nu-
 728 clei ^{137}Ba , ^{139}Ce , ^{141}Nd and ^{143}Sm has been studied in
 729 the (p,d) and $(^3\text{He},\alpha)$ neutron-removal reactions at en-
 730 ergies of 23 and 34 MeV, respectively. Relative spec-
 731 troscopic factors extracted through a DWBA analysis
 732 and centroids of single-particle strength have been estab-
 733 lished. The majority of the strength has been observed
 734 for the $s_{1/2}$ and $h_{11/2}$ orbitals. Strong fragmentation of
 735 strength was observed for the $g_{7/2}$ orbital, which is more
 736 deeply bound and significant strength lies outside of the
 737 measured excitation energy range. It proved difficult to
 738 properly disentangle $d_{3/2}$ and $d_{5/2}$ strength; the com-
 739 bined $\ell = 2$ strength distribution is broad and also seems
 740 to suffer from unobserved, presumably $d_{5/2}$, fragments.
 741 Changes in the effect of monopole shifts of neutron ener-
 742 gies due to changes in proton occupancy appear to repro-
 743 duce the trends in the effective single-particle energies of
 744 the $s_{1/2}$ and $h_{11/2}$ orbital, at least given the influence of

745 a number of other effects on the former orbital.

746 ACKNOWLEDGMENTS

747 We are grateful to John Greene (Argonne National
748 Laboratory) for his careful preparation of the $N = 82$

749 targets used in this work and to the staff at Yale for
750 their assistance in running the experiments. This work
751 was supported by the UK Science and Technology Facil-
752 ities Council and the US Department of Energy under
753 contract numbers DE-FG02-91ER-40609 and DE-AC02-
754 06CH11357.

-
- 755 [1] T. Otsuka, T. Suzuki, R. Fujimoto, H. Grawe, and 807
756 Y. Akaishi, *Phys. Rev. Lett.* **95**, 232502 (2005). 808
- 757 [2] T. Otsuka, T. Suzuki, M. Honma, Y. Utsuno, N. Tsun- 809
758 oda, K. Tsukiyama, and M. Hjorth-Jensen, *Phys. Rev.*
759 *Lett.* **104**, 012501 (2010). 810
- 760 [3] N.A. Smirnova, B. Bally, K. Heyde, F. Nowacki and 811
761 K. Sieja, *Phys. Lett. B* **686**, 109 (2010). 812
- 762 [4] J. P. Schiffer, S. J. Freeman, J. A. Caggiano, C. Deibel, 813
763 A. Heinz, C.-L. Jiang, R. Lewis, A. Parikh, P. D. Parker, 814
764 K. E. Rehm, S. Sinha and J. S. Thomas, *Phys. Rev. Lett.*
765 **92**, 162501 (2004). 815
- 766 [5] B. P. Kay, S. J. Freeman, J. P. Schiffer, J. A. Clark, 816
767 C. Deibel, A. Heinz, A. Parikh, and C. Wrede, *Phys.*
768 *Lett. B* **658**, 216 (2008). 817
- 769 [6] B. P. Kay, J. P. Schiffer, S. J. Freeman, C. R. Hoffman, 818
770 B. B. Back, S. I. Baker, S. Bedoor, T. Bloxham, J. A. 819
771 Clark, C. M. Deibel, A. M. Howard, J. C. Lighthall, S. 820
772 T. Marley, K. E. Rehm, D. K. Sharp, D. V. Shetty, J. S. 821
773 Thomas, and A. H. Wuosmaa, *Phys. Rev. C* **84**, 024325
774 (2011). 822
- 775 [7] D. K. Sharp, B. P. Kay, J. S. Thomas, S. J. Freeman, 823
776 J. P. Schiffer, B. B. Back, S. Bedoor, T. Bloxham, J. A. 824
777 Clark, C. M. Deibel, C. R. Hoffman, A. M. Howard, J. C. 825
778 Lighthall, S. T. Marley, A. J. Mitchell, T. Otsuka, P. D. 826
779 Parker, K. E. Rehm, D. V. Shetty, and A. H. Wuosmaa, 827
780 *Phys. Rev. C* **87**, 014312 (2013). 828
- 781 [8] J.P. Schiffer, C.R. Hoffman, B.P. Kay, J.A. Clark, 829
782 C.M Deibel, S.J. Freeman, A.M Howard, A.J. Mitchell, 830
783 P.D. Parker, D.K. Sharp and J.S. Thomas. *Phys. Rev.*
784 *Lett.* **108** 022501 (2012). 831
- 785 [9] J.P. Schiffer, C.R. Hoffman, B.P. Kay, J.A. Clark, 832
786 C.M Deibel, S.J. Freeman, M. Honma, A.M Howard, 833
787 A.J. Mitchell, T. Otsuka, P.D. Parker, D.K. Sharp and 834
788 J.S. Thomas. *Phys. Rev. C.* **87** 034306 (2013). 835
- 789 [10] K. Heyde and P.J. Brussard, *Z. Phys.* **259**, 15 (1973). 836
- 790 [11] R. K. Jolly and E. Kashy, *Phys. Rev. C* **4**, 887 (1971). 837
- 791 [12] R. K. Jolly and E. Kashy, *Phys. Rev. C* **4**, 1398 (1971). 838
- 792 [13] A. Chaumeaux, G. Bruge, H. Faraggi and J. Picard, 839
793 *Nucl. Phys. A* **164**, 176 (1971). 840
- 794 [14] G. Berrier, M. Vergnes, G. Rotbard and J. Kalifa, *J.*
795 *Phys. (Paris)* **37**, 311 (1976). 841
- 796 [15] S. Galès, G. M. Crawley, D. Weber and B. Zwieglinski, 842
797 *Nucl. Phys. A* **398**, 19 (1983). 843
- 798 [16] S. A. Dickey, J. J. Kraushaar, J. R. Shepard, D. W. Miller, 844
799 W. W. Jacobs and W. P. Jones, *Nucl. Phys. A* **441**, 189
800 (1985). 845
- 801 [17] C. D. Van Rooden, D. Spaargaren, H.P. Blok and J. Blok, 846
802 *Nucl. Phys. A* **430**, 125 (1984). 847
- 803 [18] K. Yagi, T. Ishimatsu, Y. Ishizaki and Y. Saji, *Nucl.*
804 *Phys. A* **121**, 161 (1968). 848
- 805 [19] J. L. Foster Jr., O. Dietzsch and D. Spalding, *Nucl. Phys.*
806 *A* **169**, 187 (1971). 849
- 807 [20] S. El-Kazzaz, J. R. Lien, G. Løvholden, P. Kleinheinz, 850
808 C. Ellegaard, J. Bjerregaard, P. Knudsen and J. Rekdal, 851
809 *Nucl. Phys. A* **280**, 1 (1977). 852
- 810 [21] J. A. Clark, Private communication (2004). 853
- 811 [22] E. Browne and J. K. Tuli, *Nuclear Data Sheets* **108**, 2173
812 (2007). 854
- 813 [23] T. W. Burrows, *Nuclear Data Sheets* **92**, 623 (2001). 855
- 814 [24] J. K. Tuli and D. F. Winchell, *Nuclear Data Sheets* **92**,
815 **277** (2001). 856
- 816 [25] J. K. Tuli, *Nuclear Data Sheets* **94**, 605 (2001). 857
- 817 [26] S.J. Freeman, D.K. Sharp, S. A. McAllister, B. P. Kay, 858
818 C. M. Deibel, T. Faestermann, R. Hertzenberger, A. J. 859
819 Mitchell, J. P. Schiffer, S. V. Szwec, J. S. Thomas, and 860
820 H.-F. Wirth, *Physical Review C* **96**, 054325 (2017). 861
- 821 [27] E. Dragulescu, M. Ivascu, R. Miha, D. Popescu, G. Seme-
822 nescu, A. Velenik and V Paar, *J. Phys. G: Nucl. Phys.*
823 **10**, 1099 (1984). 862
- 824 [28] See Supplemental Material at [URL will be inserted by
825 publisher] for detailed data on state-by-state cross sec-
826 tions and for two-body matrix elements used in calcula-
827 tions. 863
- 828 [29] S. V. Szwec, B. P. Kay, T. E. Cocolios, J. P. Entwisle, S.
829 J. Freeman, L. P. Gaffney, V. Guimares, F. Hammache,
830 P. P. McKee, E. Parr, C. Portail, J. P. Schiffer, N. de
831 Séréville, D. K. Sharp, J. F. Smith, and I. Stefan, *Phys-*
832 *ical Review C* **94**, 054314 (2016) 864
- 833 [30] B. P. Kay, T. Bloxham, S. A. McAllister, J. A. Clark, C.
834 M. Deibel, S. J. Freedman, S. J. Freeman, K. Han, A.
835 M. Howard, A. J. Mitchell, P. D. Parker, J. P. Schiffer,
836 D. K. Sharp, and J. S. Thomas, , *Physical Review C* **87**,
837 **011302(R)** (2013) 865
- 838 [31] M. H. Macfarlane and S. C. Pieper, ANL-76-11 Rev. 1,
839 ANL Report (1978). 866
- 840 [32] S.V. Szwec, B.P. Kay, T.E. Cocolios, J.P. Entwisle,
841 S.J. Freeman, L.P. Gaffney, V. Guimarães, F. Ham-
842 mache, P.P. McKee, E. Parr, C. Portail, J.P. Schiffer,
843 N. de Séréville, D.K. Sharp, J.F. Smith, and I. Stefan,
844 *Phys. Rev. C* **94** 054314, (2016). 867
- 845 [33] R.B. Wiringa, V.G.J Stoks and R. Schiavilla, *Phys. Rev.*
846 *C* **51** 38, (1995). 868
- 847 [34] I. Brida, S.C. Pieper and R.B. Wiringa, *Phys. Rev. C* **84**
848 **024319**, (2011). 869
- 849 [35] A.J. Koning and J.P. Delaroche, *Nucl. Phys. A* **713**, 231
850 (2003). 870
- 851 [36] C. M. Perey, and F. G. Perey, *Phys. Rev.* **132**, 755 (1963). 871
- 852 [37] D.Y. Pang, P. Roussel-Chomaz, H. Savajols, R.L. Varner
853 and R. Wolski, *Phys. Rev. C* **79** 024615, (2009). 872
- 854 [38] H. An and C. Cai, *Phys. Rev. C* **73** 054605, (2006). 873
- 855 [39] G. Bassani and J Picard, *Nucl. Phys. A* **131**, 653 (1969). 874
- 856 [40] M. H. Macfarlane and J. B. French, *Rev. Mod. Phys.* **32**,
857 **567** (1960). 875
- 858 [41] L. Lapikàs, Nucl. Phys. A553, 297 (1993) *Nucl. Phys.*

- 859 [A553, 297 \(1993\)](#).
860 [42] G. J. Kramer, H. P. Blok, and L. Lapikàs, [Nucl. Phys.](#)
861 [A679, 267 \(2003\)](#). *Nucl. Phys.*
862 [43] B.P. Kay, J.P. Schiffer and S.J. Freeman, [Phys. Rev. Lett.](#)
863 [111 042502 \(2013\)](#).
864 [44] J.E. Park, W.W. Daehnick and M.J. Spisak, [Phys. Rev.](#)
865 [C 15 587, \(1977\)](#).
866 [45] J.C Veefkind, D. Spaargaren, J. Blok and K. Heyde, [Z.](#)
867 [Physik A 275 55, \(1975\)](#).
868 [46] J.P. Schiffer, Chapter 13 Isospin in Transfer Reactions,
869 in Isospin in Nuclear Physics, edited by D.H. Wilkinson
870 (Elsevier 1969).
871 [47] B. H. Wildenthal, E. Newman, and R. L. Auble, [Phys.](#)
872 [Rev. C 3, 1199 \(1971\)](#).
873 [48] W.P. Jones, L.W. Borgman, K.T. Hecht, John Bardwick
874 and W.C. Parkinson, [Phys. Rev. C 4, 508 \(1971\)](#).
875 [49] J. P. Entwisle, B. P. Kay, A. Tamii, S. Adachi, N. Aoi, J.
876 A. Clark, S. J. Freeman, H. Fujita, Y. Fujita, T. Furuno,
877 T. Hashimoto, C. R. Hoffman, E. Ideguchi, T. Ito, C.
878 Iwamoto, T. Kawabata, B. Liu, M. Miura, H. J. Ong, J.
879 P. Schiffer, D. K. Sharp, G. Süsoy, T. Suzuki, S. V. Szewc,
880 M. Takaki, M. Tsumura, and T. Yamamoto, [Phys. Rev.](#)
881 [C 93, 064312 \(2016\)](#).
882 [50] John P. Schiffer and William W. True, [Rev. Mod. Phys.](#)
883 [48, 191 \(1976\)](#).
884 [51] A. Bohr and B.R. Mottelson, *Nuclear Structure* (W.A.
885 Benjamin Inc., New York, 1969) Vol 1 p. 238.
886 [52] C.R. Hoffman, B.P. Kay and J.P. Schiffer, [Phys. Rev. C](#)
887 [89, 061305\(R\) \(2014\)](#).
888 [53] A. Hosaka, K.I Kubo and H. Toki, [Nucl. Phys. A444, 76](#)
889 [\(1985\)](#).
890 [54] A. Etchegoyen, M.C. Etchegoyen and E.G. Vergini, [Com-](#)
891 [puter Physics Communications 55, 227 \(1989\)](#).
892 [55] E. Teruya, N. Yoshinaga, K. Higashiyama and A. Oda-
893 hara, [Phys. Rev. C 92, 034320 \(2015\)](#).
894 [56] K. Higashiyama and N. Yoshinaga, [Phys. Rev. C 83,](#)
895 [034321 \(2011\)](#).